Physical Nature of Surface Structure Degradation in Long Term Operated Rails

V. E. Gromov[1,a)], A. A. Yuriev[2,b)], O. A. Peregudov[1,c)], S. V. Konovalov[3,d)], Yu. F. Ivanov[4,5,e)], A. M. Glezer[6,f)], and A. P. Semin[1,g)]

[1] *Siberian State Industrial University, Novokuznetsk, 654007 Russia*
[2] *JSC EVRAZ, Consolidated West Siberian Metallurgical Plant, Novokuznetsk, 654043 Russia*
[3] *Samara National Research University, Samara, 443086 Russia*
[4] *Tomsk National Research State University, Tomsk, 634050 Russia*
[5] *Institute of High Current Electronics SB RAS, Tomsk, 634021 Russia*
[6] *I. P. Bardin Central Research Institute of Ferrous Metallurgy, Moscow, 105005 Russia*

[a)] Corresponding author: gromov@physics.sibsiu.ru
[b)] Ant-yurev@yandex.ru
[c)] olegomgtu@mail.ru
[d)] ksv@ssau.ru
[e)] yufi55@mail.ru
[f)] a.glezer@mail.ru
[g)] syomin53@gmail.com

Abstract. Here we present research data on the structural-phase state and surface properties of rails after long-term operation with a transported tonnage of gross weight 500 and 1000 mln tons. Using optical, scanning, and transmission electron diffraction microscopy, and measurements of microhardness and tribological parameters, it is shown that the wear rate of the material after transport of 500 and 1000 mln tons increases 3 and 3.4 times, respectively, and the friction coefficient decreases 1.4 and 1.1 times. After transport of 500 mln tons, complete failure of cementite plates occurs resulting in round cementite particles of size 10–50 nm. After transport of 1000 mln tons, dynamic recrystallization develops in the material. Two competitive mechanisms are suggested for such evolution: (1) decomposition of cementite particles with their transfer to the volume of ferrite grains or plates in pearlite and (2) decomposition and dissolution of cementite particles, transition of carbon atoms to dislocations (to Cottrell atmospheres), transfer of carbon atoms by dislocations to the volume of ferrite grains or plates, and formation of nano-sized cementite particles.

INTRODUCTION

The increasing traffic volume and density on railways causes early failure of rails because of different factors, including contact fatigue. Up to 15% of all rails for replacement show impermissible rates of wear or crushing [1]. As well as being a matter of practical concern, the problem of rail fracture is a subject of research interest in physical materials science [2]. The wear of rails is the key parameter that determines their service life on railways with high traffic density. When the surface of rails is involved in severe plastic deformation, cementite plates are either bent or fractured and extremely high dislocation densities arise at interphase boundaries, resulting in cementite dissolution and austenite formation due to reverse $\alpha \rightarrow \gamma$ transformation [3–9].

Cementite is normally very stable and its strain-induced decomposition indicates that it comes out of phase equilibrium. For understanding the processes that drive this compound and hence other phases out of balance, we should carefully analyze how structural-phase states and defect substructures evolve under severe (mega) plastic deformation [5–7, 9, 10].

Proceedings of the International Conference on Advanced Materials with Hierarchical Structure for New Technologies and Reliable Structures 2017 (AMHS'17)
AIP Conf. Proc. 1909, 020066-1–020066-4; https://doi.org/10.1063/1.5013747
Published by AIP Publishing. 978-0-7354-1601-7/$30.00

TABLE 1. Tribological data for rail tread surface

State	Friction coefficient, μ	Wear rate, 10^{-5}, mm^3/Nm
Initial	0.49	3.2
500 mln t	0.36	9.8
1000 mln t	0.43	10.9

Our aim here is to analyze the evolution of surface properties, structure, phase composition, and defect substructure of long operated rails.

MATERIALS AND RESEARCH TECHNIQUES

For our study we used specimens cut out of steel rails (GOST R 51685-2000) as received (fresh) and after operation on railways with a transported tonnage of gross weight 500 and 1000 mln tons. The metal structure was examined by metallography (etching in a 4% ethanol solution with nitric acid), scanning electron microscopy (fractography), and transmission (thin foil) electron diffraction microscopy [11–13]. The specimens for shock loading were cut from the middle of a rail head so that the running surface would be in the plane above a stress concentrator. The foils for transmission microscopy were electrolytically thinned plates spark cut directly from the running surface and at 2 and 10 mm away from.

The surface strength of the specimens was analyzed using a PMT-3 microhardness tester with a Vickers pyramid, and their friction coefficient and wear rate were analyzed using a Tribotechnic tribometer (France) with a quenched steel ball of diameter 3 mm (stationary counterbody) at a linear rotation rate of 2.0–2.5 cm/s and load of 10 N; the number of rotations was 5000. After tests, the friction groove profile, depth, and cross-sectional area were estimated. The wear resistance was estimated as the inverse of wear intensity or specific wear rate calculated by the formula

$$V = \frac{2\pi RA}{FL} \ [\mathrm{mm^3/N\,m}],$$

where R is the track radius [mm], A is the wear groove cross-sectional area [mm^2], F is the applied load [N], and L is ball travel distance [m].

RESULTS AND DISCUSSION

For the initial rail specimens, we determined the relative content of lamellar pearlite (~0.7), ferrite-carbide grains (~0.25), and free ferrite grains (~0.05). More data, in addition to those reported below, on the state of rails after transport of 500 mln tons can be found elsewhere [14–17] and after transport of 1000 mln tons elsewhere [18–21].

Changes along the central axis and fillet after transport of tonnage 500 mln tons. First, let us dwell on the changes along the central axis. As can be seen from tribological data in Table 1, the service of rails greatly decreases their wear resistance. After transport of tonnage with a gross weight of 500 mln, their wear resistance at the tread surface decreases three times with attendant decrease in the friction coefficient and their surface hardness measures ~7.0 GPa. With distance from the tread surface, the metal hardness decreases reaching a plateau at 10–12 mm.

Their fracture surface reveals three characteristic zones: a zone of normal crack growth, a zone of accelerated crack growth, and a zone of rupture. So, the fracture mechanism is mixed. On the fracture surface, there are ductile dimples and cleavage facets. The dimples dominate in the structure and result from micropores through which fracture develops.

During operation, the rail steel greatly changes its surface structure. After transport of 500 mln tons, cementite plates in pearlite colonies fail completely (Fig. 1). In the volume of lamellar pearlite, round cementite particles appear measuring 30–50 nm (Fig. 1a) and 10–15 nm (Fig. 1b). The failure of cementite plates involves fragmentation of ferrite in pearlite to an average size of 150 nm (Fig. 1a). In the volume of fragments, one can observe a dislocation substructure with a scalar dislocation density reaching 1×10^{11} cm^{-2}.

The data suggest two competitive mechanisms developing in the steel during its operation: (1) decomposition of cementite particles and their transfer to the volume of ferrite grains or plates of pearlite and (2) decomposition and dissolution of cementite particles, transition of carbon atoms to dislocations (to Cottrell atmospheres), transfer of carbon atoms by dislocations to the volume of ferrite grains (or plates), and repeated formation of nano-sized cementite particles.

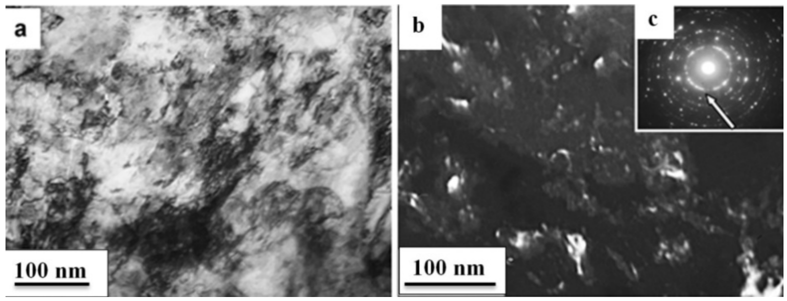

FIGURE 1. Surface structure of rail steel: a—bright field; b—dark field in reflection [112} Fe3C; c—electron diffraction pattern; arrow indicates reflection for dark field

Analysis of the changes along the fillet shows the following. While the hardness of the rail steel during operation increases along the central axis, its surface layer becomes softer. After long-term operation, the surface layer of the rail steel reveals substantial structural-phase transformation. The lamellar morphology of pearlite changes via dissolving cementite plates with the formation of chains of globular carbide particles at their sites, which is due to carbon atoms escaped from the cementite lattice to dislocations. Then, nano-sized carbide particles arise in the ferrite interlayers of pearlite. The ferrite-carbide mixture evolves with the formation of a fragmented substructure consisting of fragments (subgrains) of size 250–300 nm in the volume and at the boundaries of which second-phase particles are located. Judging from electron diffraction patterns, these are iron carbide particles; in some cases, iron oxides are detected.

At a depth of 2 mm, the substructure of the rail steel reveals the following transformation. First, the scalar dislocation density in the ferrite volume increases 0.5 to 2.0 times. Second, the lamellar cementite phase is fragmented and decomposed. Third, nano-sized carbide particles are formed in the ferrite component of the steel. Nano-sized particles are found in the grains of pearlite, ferrite-carbide mixture, and free ferrite.

The main sources of lattice bending-torsion, no matter what the distance to the tread surface, are cementite and ferrite interfaces. As the rail fillet surface is approached, the number of bend extinction contours (stress concentrators) per unit surface area increases and their transverse dimension decreases (long-range internal stress fields increase in amplitude).

Changes along the central axis and fillet after transport of tonnage 1000 mln tons. After transport of 1000 mln tons, like 500 mln tons, the wear resistance of the tread surface decreases with a slight decrease in the friction coefficient. In a near-surface layer ~2 mm thick, the hardness decreases two times compared to its value at a depth of ~10 mm, suggesting that the material structure degrades during operation.

Comparison shows that the thickness of the rupture zone depends almost not at all on the tonnage transported. In the rupture zone, one can identify a surface sublayer of up to 40 μm thick with a large number of cracks, micropores of size 1–2 μm, and dints. Such fracture causes separation of the surface layer from the material volume.

After transport of 500 mln tons, the volume of ferrite grains assumes a band substructure, and after transport of 1000 mln tons, it is dominated by a subgrain structure, which likely evidences the onset of dynamic recrystallization. In the subgrain volume, chaotically distributed dislocations with a scalar density no greater than 10^8 cm^{-2} are detected. Another distinctive feature is the appearance of a structure with specific reflections on electron diffraction patterns: individual points of α phase (solid solution based in bcc Fe) with a large number of thin diffraction rings which most likely belong to nano-sized carbide and oxycarbide particles.

The transformation of ferrite-carbide grains results in a fragmented (subgrain) structure with redistributed cementite particles: whereas the initial steel features almost uniform distribution of globular cementite particles over the ferrite-carbide grain volume, their location at ~2 mm from the tread surface falls mostly on subgrain boundaries. Two mechanisms can be suggested for the formation of such structure: first, the subboundaries may arise in the region of carbide particles, and second, the particles residing in the volume may dissolve and precipitate at the subgrain boundaries.

As for the changes along the fillet, we can note a considerable (1.5–2.0 times) increase in the microhardness of a layer ~10 mm thick and evident surface strengthening, which is also observed for a tonnage of 500 mln tons.

The surface structure is dominated by fragmented substructure with a fragment (subgrain) size of 100–150 nm. Its electron diffraction pattern reveals quasi-rings, which is also indicative of the nano-sized surface state. The fragment boundaries are decorated by round second-phase particles of size 15–20 nm. Analysis shows that these are Fe carbide particles; in some cases, reflections of Fe oxides are detected.

After transport of 1000 mln tons, the structure at a depth of 2 mm from the rail surface fillet becomes highly heterogeneous. First, there are lamellar pearlite grains with misoriented ferrite regions; a similar structure is formed in ferrite-carbide grains. Second, there are pearlite grains and ferrite-carbide grains with partially or completely dissolved cementite plates at the site of which round carbide particles of size 15–30 nm arise. Third, there are grains of free ferrite with a subgrain structure. At ~10 mm from the fillet surface, the steel rail structure is close in morphology and phase composition to its state before service.

CONCLUSION

Thus, we have investigated the structural-phase state, microhardness, and tribological properties of rails along their central axis and fillet after long-term operation (transported tonnage of gross weight 500 and 1000 mln tons). During operation, the surface layers of the rail steel with lamellar pearlite grains are fractured with the formation of nano-sized ferrite-carbide particles. After transport of 500 mln tons, complete failure of cementite plates occurs resulting in round cementite particles of size 10–50 nm. After transport of 100 mln tons, dynamic recrystallization develops in the material. The wear rate after transport of 500 and 1000 mln tons increases 3 and 3.4 times, respectively, and the friction coefficient decreases 1.4 and 1.1 times. Two possible mechanisms are suggested for such evolution: (1) decomposition of cementite particles with their transfer to the volume of ferrite grains or plates in pearlite and (2) decomposition and dissolution of cementite particles, transition of carbon atoms to dislocations (to Cottrell atmospheres), transfer of carbon atoms by dislocations to the volume of ferrite grains or plates, and formation of nano-sized cementite particles.

This work was supported by the Russian Science Foundation (project No. 15-12-00010).

REFERENCES

1. E. A. Shur, *Rail Damage* (Intekst, Moscow, 2012).
2. V. E. Gromov, A. B. Yuriev, K. V. Morozov, and Yu. F. Ivanov, *Microstructure of Hardened Rails* (Inter-Kuzbass, Novokuznetsk, 2014).
3. Yu. Ivanisenko and H. J. Fecht, Steel Tech. **3**, 19–23 (2008).
4. Yu. Ivanisenko, I. MacLaren, X. Sauvage, R. Z. Valiev, and H.-J. Fecht, Acta Mater. **54**, 1659–1669 (2006).
5. Ning Jiang-li, E. Courtois-Manara, L. Kurmanaeva, A. V. Ganeev, R. Z. Valiev, C. Kübel, and Yu. Ivanisenko, Mater. Sci. Eng. A **581**, 8–15 (2013).
6. V. G. Gavriljuk, Mater. Sci. Eng. A **345**, 81–89.
7. Y. J. Li, P. Chai, C. Bochers, S. Westerkamp, S. Goto, D. Raabe, and R. Kirchheim, Acta Mater. **59**, 3965–3977 (2011).
8. V. G. Gavriljuk, Scripta Mater. **45**, 1469–1472 (2001).
9. A. M. Glezer, Bull. Russ. Acad. Sci. Phys. **71**, 1722 (2007).
10. V. E. Gromov, E. V. Kozlov, V. I. Bazaikin, et al., *Physics and Mechanics of Drawing and Forging* (Nedra, Moscow, 1997).
11. G. Thomas and M. J. Goringe, *Transmission Electron Microscopy of Materials* (Wiley, New York).
12. P. B. Hirsch, A. Howie, R. B. Nicholson, D. W. Pashley, and M. J. Whelan, *Electron Microscopy of Thin Crystals* (Butterworth, Washington).
13. L. M. Utevskii, *Diffraction Electron Microscopy in Metallography* (Metallurgia, Moscow, 1973).
14. Yu. F. Ivanov, V. E. Gromov, O. A. Peregudov, K. V. Morozov, and A. B. Yuriev, Steel Trans. **45**, 254–257 (2015)
15. O. A. Peregudov, V. E. Gromov, Yu. F. Ivanov, K. V. Morozov, K. V. Alsaraeva, and O. A. Semina, AIP Conf. Proc. **1683**, 4 p. (2015).
16. Yu. F. Ivanov, O. A. Peregudov, K. V. Morozov, V. E. Gromov, N.A. Popova, and E. N. Nikonenko, IOP Conf. Mater. Sci. Eng. **112**, 4 p. (2016).
17. V. E. Gromov, O. A. Peregudov, Y. F. Ivanov, A. M. Glezer, K. V. Morozov, K. V. Aksenova, and O. A. Semina, AIP Conf. Proc. **1783**, 020069 (2016).
18. Yu. F. Ivanov, O. A. Peregudov, K. V. Morozov, V. E. Gromov, N. A. Popova, and E. N. Nikonenko, IOP Conf. Mater. Sci. Eng. **112**, 4 p. (2016).
19. O. A. Peregudov, V. E. Gromov, Y. F. Ivanov, K. V. Morozov, and S. V. Konovalov, Steel Trans. **46**, 260–263 (2016).
20. O. A. Peregudov, K. V. Morozov, V. E. Gromov, A. M. Glezer, and Yu. F. Ivanov, Russ. Metall. **2016**, 371–374 (2016).
21. V. E. Gromov, Y. F. Ivanov, K. V. Morozov, O. A. Peregudov, and O. A. Semina, J. Surf. Invest. X-ray Synchrotron Neutron Tech. **10**, 1101–1105 (2016).